

Bound isoscalar axial-vector $bc\bar{u}\bar{d}$ tetraquark T_{bc} from lattice QCD using two-meson and diquark-antidiquark variational basis

M. Padmanath,^{1,*} Archana Radhakrishnan,^{2,†} and Nilmani Mathur^{2,‡}

¹*The Institute of Mathematical Sciences, a CI of Homi Bhabha National Institute, Chennai, 600113, India*

²*Department of Theoretical Physics, Tata Institute of Fundamental Research, Homi Bhabha Road, Mumbai 400005, India*

(Dated: May 2, 2024)

We report a lattice QCD study of the heavy-light meson-meson interactions with an explicitly exotic flavor content $bc\bar{u}\bar{d}$, isospin $I=0$, and axialvector $J^P = 1^+$ quantum numbers in search of possible tetraquark bound states. The calculation is performed at four values of lattice spacing, ranging ~ 0.058 to ~ 0.12 fm, and at five different values of valence light quark mass $m_{u/d}$, corresponding to pseudoscalar meson mass M_{ps} of about 0.5, 0.6, 0.7, 1.0, and 3.0 GeV. The energy eigenvalues in the finite-volume are determined through a variational procedure applied to correlation matrices built out of two-meson interpolating operators as well as diquark-antidiquark operators. The continuum limit estimates for $D\bar{B}^*$ elastic S -wave scattering amplitude are extracted from the lowest finite-volume eigenenergies, corresponding to the ground states, using amplitude parametrizations supplemented by a lattice spacing dependence. Light quark mass $m_{u/d}$ dependence of the $D\bar{B}^*$ scattering length (a_0) suggests that at the physical pion mass $a_0^{phys} = +0.57(^{+4}_{-5})(17)$ fm, which clearly points to an attractive interaction between the D and \bar{B}^* mesons that is strong enough to host a real bound state T_{bc} , with a binding energy of $-43(^{+6}_{-7})(^{+14}_{-24})$ MeV with respect to the $D\bar{B}^*$ threshold. We also find that the strength of the binding decreases with increasing $m_{u/d}$ and the system becomes unbound at a critical light quark mass $m_{u/d}^*$ corresponding to $M_{ps}^* = 2.73(21)(19)$ GeV.

The discovery of a doubly charmed tetraquark¹, T_{cc} , marks an important milestone [1] in spectroscopy of hadrons. Phenomenologically, doubly heavy tetraquarks in the heavy quark limit are long hypothesized to form deeply bound states [2–12] with binding energy $\mathcal{O}(100)$ MeV with respect to the elastic strong decay threshold. While doubly bottom tetraquarks are suitable candidates for such deeply bound states, as predicted by multiple lattice QCD calculations [13–18], T_{cc} is found to be 360 keV below the lowest two-meson threshold ($D^0 D^{*+}$). A handful of recent experimental developments involving multiple heavy quark production such as the recent discoveries of Ξ_{cc} [19], T_{cc} [1], reports of tri- J/ψ [20], associated $J/\psi\Upsilon$ [21], and di- Υ [22] productions, and recent proposals of inclusive search strategies [23, 24] augment promising prospects for the doubly heavy hadron sector in the near future. In light of these advancements, a doubly heavy tetraquark with a bottom and a charm quark with a valence quark configuration $T_{bc} \equiv bc\bar{u}\bar{d}$ is going to be one of the most sought-after hadron in this decade [25]. In this work, using lattice QCD calculations, we show a clear evidence of an attractive interaction between the D and \bar{B}^* mesons that is strong enough to host a real bound state T_{bc} . This finding will further boost the search for such bottom-charm tetraquarks.

The phenomenological picture on deeply bound doubly

heavy tetraquarks is based on a compact heavy diquark-light antidiquark interpretation [14, 26], whereas the shallow binding energy of T_{cc} could possibly be a reflection of its dominant noncompact molecular nature [8, 27]. Bottom-charm tetraquarks form an intermediate platform, where there could be complicated interplay between these pictures. A collective and refined knowledge of the low energy spectra in all these three doubly heavy systems (T_{bb} , T_{bc} and T_{cc}) could culminate in a deeper understanding of strong interaction dynamics across a wide quark mass regime spanning from charm to the bottom quarks. The isoscalar bottom-charm tetraquarks with quantum numbers $[I(J^P) = 0(1^+)]$ have been investigated previously both using lattice [28–30] and nonlattice methodologies [5, 6, 8, 9, 11, 12, 26, 31–40]. The predictions from nonlattice approaches are quite scattered from being unbound to deeply bound, whereas the difference in conclusions from the three existing lattice QCD investigations [28–30] call for more detailed efforts in this regard.

In this work, we perform a lattice QCD simulation of coupled $D\bar{B}^*$ and $\bar{B}D^*$ two-meson channels² that are the relevant lowest two strong decay thresholds, in the order of increasing energies, $E_{D\bar{B}^*} = M_{\bar{B}^*} + M_D$ and $E_{\bar{B}D^*} = M_{\bar{B}} + M_{D^*}$, where M_h is the mass of the hadron h . The extracted finite-volume ground state energies are utilized to constrain the continuum extrapolated elastic

¹ We follow the nomenclature that a “tetraquark” refers to any bound state or resonance with dominant four-quark Fock component, whether it is a compact four-quark object or a two-meson molecule or a mixture of both.

² We work in the isosymmetric limit with no QED effects and $m_u = m_d$. Hence we choose to call the degenerate $(D^+ B^-)$, $(D^0 \bar{B}^0)$ threshold as $D\bar{B}$, and equivalently for others like $D\bar{B}^*$, $\bar{B}D^*$ and $D^* \bar{B}^*$.

$D\bar{B}^*$ scattering amplitudes following the Lüscher's finite-volume prescription [41, 42]. The light quark mass $m_{u/d}$ dependence of the extracted amplitudes suggests a binding energy of $-43^{(+6)}_{(-7)}(-14)^{(+14)}_{(-24)}$ MeV for the $bc\bar{u}\bar{d}$ tetraquark pole with respect to $E_{D\bar{B}^*}$ at the physical point $m_{u/d}^{phys}$.

Label	Symbol	a [fm]	$N_s^3 \times N_t$	M_{ps}^{sea}
S_1	$\color{red}\blacklozenge$	0.1207(11)	$24^3 \times 64$	305
S_2	$\color{violet}\blacklozenge$	0.0888(8)	$32^3 \times 96$	312
S_3	$\color{blue}\bullet$	0.0582(4)	$48^3 \times 144$	319
L_1	$\color{green}\blacksquare$	0.1189(9)	$40^3 \times 64$	217

TABLE I. Relevant details of the lattice QCD ensembles used. The lattice spacing estimates are measured using the r_1 parameter [43]. L_1 refers to large spatial volume, and S_1 , S_2 , and S_3 refer to small spatial volumes.

Lattice setup: We use four lattice QCD ensembles (see Table I for relevant details) with $N_f = 2+1+1$ dynamical Highly Improved Staggered Quark (HISQ) fields generated by the MILC collaboration [43]. The charm and strange quark masses in the sea are tuned to their respective physical values, whereas the dynamical light quark masses correspond to sea pion masses as listed in Table I. We utilize a partially quenched setup on these configurations with valence quark fields up to the charm quark masses realized using an overlap fermion action as in Refs. [44, 45]. We employ a nonrelativistic QCD (NRQCD) Hamiltonian [46] for the bottom quark. Following the Fermilab prescription [47], the bare charm [48, 49] and bottom [50] quark masses on each ensemble are tuned using the kinetic mass of spin averaged $1S$ quarkonia $\{a\bar{M}_{kin}^{QQ} = \frac{3}{4}aM_{kin}(V) + \frac{1}{4}aM_{kin}(PS)\}$ determined on the respective ensembles. The bare strange quark mass is set by equating the lattice estimate for the fictitious pseudoscalar $\bar{s}s$ meson mass to 688.5 MeV [51].

For the valence $m_{u/d}$, we investigate five different cases: three unphysical quark masses [corresponding to approximate pseudoscalar meson masses $M_{ps} \sim 0.5, 0.6$, and 1.0 GeV], the strange quark mass [$M_{ps} \sim 0.7$ GeV] and the charm quark mass [$M_{ps} \sim 3.0$ GeV]. We evaluate the finite-volume spectrum for all these five quark masses on all four ensembles, investigate the scattering of D and \bar{B}^* mesons in all five cases and then extract the $m_{u/d}$ (otherwise M_{ps}) dependence of the scattering parameters.

Interpolators and measurements: The finite-volume spectrum is determined from Euclidean two-point correlation functions $\mathcal{C}_{ij}(t)$, between interpolating operators $\mathcal{O}_{i,j}(\mathbf{x}, t)$ with desired quantum numbers, given by

$$\mathcal{C}_{ij}(t) = \sum_{\mathbf{x}} \langle \mathbb{O}_j^\dagger(0) \mathcal{O}_i(\mathbf{x}, t) \rangle \approx \sum_n Z_j^{n\dagger} Z_i^n e^{-E^n t}. \quad (1)$$

Here E^n is the energy of the n^{th} state and $Z_i^n = \langle 0 | \mathcal{O}_i | n \rangle$ is the operator-state overlap between the sink operator \mathcal{O}_i and state n . We use \mathbb{O} and \mathbb{Z} to represent the

source operator and overlaps to distinguish them from that for the sink as we follow a wall-source to point-sink construction in our \mathcal{C}_{ij} evaluations. This is well-established procedure in ground state energy determination, despite the non-Hermitian setup in Eq. (1) (see Refs. [14, 16, 28, 29, 52, 53] for details). We use the following set of linearly independent, yet Fierz related [54], operators,

$$\begin{aligned} \mathcal{O}_1(x) &= [\bar{u}(x)\gamma_i b(x)][\bar{d}(x)\gamma_5 c(x)] \\ &\quad - [\bar{d}(x)\gamma_i b(x)][\bar{u}(x)\gamma_5 c(x)] \\ \mathcal{O}_2(x) &= [\bar{u}(x)\gamma_5 b(x)][\bar{d}(x)\gamma_i c(x)] \\ &\quad - [\bar{d}(x)\gamma_5 b(x)][\bar{u}(x)\gamma_i c(x)] \\ \mathcal{O}_3(x) &= (\bar{u}(x)^T \Gamma_5 \bar{d}(x) - \bar{d}(x)^T \Gamma_5 \bar{u}(x))(b(x)\Gamma_i c(x)). \end{aligned} \quad (2)$$

\mathcal{O}_1 and \mathcal{O}_2 are two-meson operators of the type $D\bar{B}^*$ and $\bar{B}D^*$, respectively. \mathcal{O}_3 is a diquark-antidiquark type operator. Here $\Gamma_k = C\gamma_k$ with $C = i\gamma_2\gamma_4$ being the charge conjugation matrix and the diquarks (antidiquarks) in the color antitriplet (triplet) representations. Other high lying two-meson ($D^*\bar{B}^*$) and three-meson ($D\bar{B}\pi$) interpolators are ignored in this analysis as they are sufficiently high in energy to have any effects on the extracted ground states. Bilocal two-meson interpolators with nonzero internal meson momenta are also not considered, which would be an important step ahead [55]. We also compute two-point correlation functions for \bar{B} , \bar{B}^* , D , and D^* mesons, using standard local quark bilinear interpolators ($\bar{q}\Gamma Q$) with spin structures $\Gamma \sim \gamma_5$ and γ_i for pseudoscalar and vector quantum numbers, respectively.

Analysis: The correlation matrices \mathcal{C} evaluated for the basis in Eq. (2) are analyzed following a variational procedure [56] by solving the generalized eigenvalue problem (GEVP), $\mathcal{C}(t)v^n(t) = \lambda^n(t)\mathcal{C}(t_0)v^n(t)$. The eigenvalues in the large time limit represent the time evolution of the low lying eigenenergies \mathcal{E}^n as $\lim_{t \rightarrow \infty} \lambda^n(t) \sim A_n e^{-\mathcal{E}^n t}$. The corresponding eigenvectors $v^n(t)$ are related to the operator-state-overlaps Z_i^n .

Eigenenergy extraction proceeds via fitting the eigenvalue correlators, $\lambda_n(t)$, or the ratios $R^n(t) = \lambda^n(t)/\mathcal{C}_{m_1}(t)\mathcal{C}_{m_2}(t)$, with the expected asymptotic exponential behaviour. Here, \mathcal{C}_{m_i} is the two-point correlation function for the meson m_i . $R^n(t)$ is empirically known to efficiently mitigate correlated noise between the product of two single hadron correlators and the interacting correlator for the two-hadron system [57]. Note that the automatic cancellation of the additive quark mass offset, inherent to NRQCD formulation, is an added advantage in using $R^n(t)$ for the fits. The systematics associated with the chosen time interval for fitting are assessed by varying the lower boundary of the time interval, t_{min} , with a fixed upper boundary, t_{max} , chosen considering the noise level. In Figure 1, we present a representative plot showing this t_{min} dependence of the energy splittings ($\Delta\mathcal{E}^n$) determined from the fits to $\lambda^n(t)$ and $R^n(t)$, respectively. The energy differences are evaluated from $\lambda^n(t)$

using the relation $\Delta\mathcal{E}^n = \mathcal{E}^n - M_{m_1} - M_{m_2}$, whereas the fits to $R^n(t)$ directly yield the respective estimates. We choose the optimal t_{min} values where the two different procedures found to agree asymptotically in time. We also perform additional checks considering an alternative quark smearing with different smearing widths to affirm our energy estimates, see Appendix A. Our final results are based on fitting the ratio correlators $R^n(t)$.

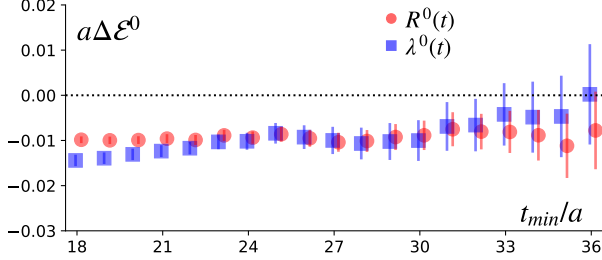


FIG. 1. t_{min} dependence of the $\Delta\mathcal{E}^0$ fit estimates determined from the fits to λ^0 and $R^0(t)$ for the case $M_{ps} \sim 700$ MeV in the finest ensemble. Here the superscript 0 refers to the lowest eigenenergy.



FIG. 2. The GEVP eigenenergies in finite-volume for isoscalar axialvector $bc\bar{u}\bar{d}$ channel on the L_1 ensemble. Five panels show the results obtained at various pseudoscalar meson masses (M_{ps}) 0.5, 0.6, 0.7, 1.0, and 3.0, respectively.

Finite-volume eigenenergies: In Figure 1, we present the finite-volume GEVP eigenenergies, in lattice units, for the isoscalar axialvector $bc\bar{u}\bar{d}$ channel. The results shown are for the L_1 ensemble at the five different $m_{u/d}$ values corresponding to $M_{ps} \sim 0.5, 0.6, 0.7, 1.0$, and 3.0 GeV. Note that these estimates include the additive offsets related to the NRQCD-based bottom quark dynamics. The non-interacting two-meson energy levels corresponding to $D\bar{B}^*$ and $\bar{B}D^*$ thresholds are indicated as dotted horizontal line segments and those related to \bar{B}^*D^* threshold by dashed lines for each M_{ps} . The lowest eigenenergy or the ground state energy is dominated by the Z_1^0 factor corresponding to \mathcal{O}_1 , that is related to the $D\bar{B}^*$ threshold and is determined unambiguously by the operator \mathcal{O}_1 , see Ref. [58] for details. The most important observation is a clear trend for negative energy shifts in the ground state energies, which can be observed in all the cases, indicating a possible attractive interaction between the D and \bar{B}^* mesons [59]. A similar pattern of low lying

eigenenergies and ground state negative energy shifts are also observed in other ensembles, see details in Ref. [58]. We expect that for our choice of interpolating operators and the accessible values of t , \mathcal{E}^0 will be an accurate estimate of E^0 , whereas our setup is unable to accurately estimate excited-state energies. This means the excited eigenenergies presented in Figure 1 may not correspond to the higher lying elastic excitations of the $D\bar{B}^*$ channel. The location of lowest two non-interacting finite-volume levels related to the $D\bar{B}^*$ channel along with the ground state eigenenergies are presented in Appendix B. Hence we focus only on the ground state energies ($\mathcal{E}^0 \sim E^0$) for the rest of the analysis.

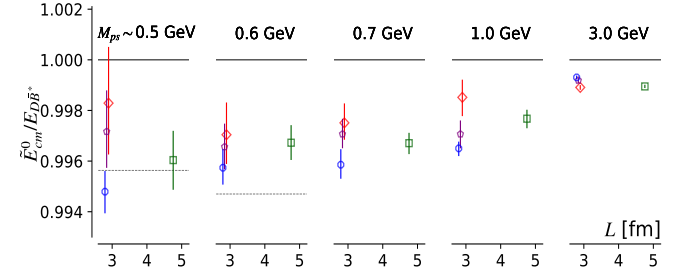


FIG. 3. The ground state energies in units of $E_{D\bar{B}^*}$ on all ensembles (see Table I for color-symbol conventions) for all M_{ps} values (different vertical panels).

In Figure 3, we present the ground state energy estimates, in units of $E_{D\bar{B}^*}$, at various M_{ps} and for all the ensembles. These estimates are evaluated as $E^n = \Delta E^n + M_D + \tilde{M}_{\bar{B}^*}$, where ΔE^n is the estimate from fit to $R^n(t)$, $\tilde{M}_{\bar{B}^*} = M_{\bar{B}^*} - 0.5\bar{M}_{lat}^{bb} + 0.5\bar{M}_{phys}^{bb}$ accounts for the NRQCD additive offset, and $\bar{M}_{lat}^{bb}(\bar{M}_{phys}^{bb})$ refers to the spin averaged mass of the $1S$ bottomonium measured on the lattice (experiments). The eigenenergies clearly show a trend of decreasing energy splitting, hence decreasing interaction strength, with increasing M_{ps} . Another interesting feature to note here is the nonzero lattice spacing (a) dependence of the ground state energies on similar volume ensembles (S_1, S_2, S_3), which we account for through an a dependence in the parametrized amplitude as discussed below.

In Figure 3, we also indicate the branch point location of the left hand cut (lhc) arising out of an off-shell pion exchange process for different M_{ps} by horizontal dashed lines. Recent developments point to the importance of lhc effects on virtual subthreshold poles related to the T_{cc} tetraquark [60]. Such effects on bound states are the subject of future studies where one could successfully solve the relevant three particle integral equations. This is beyond the scope of this work and we ignore such effects in our analysis.

$D\bar{B}^$ scattering amplitude:* Assuming these energy splittings in ground states are purely described by elastic scattering in the $D\bar{B}^*$ system, we utilize them to con-

strain the associated S -wave scattering amplitude following Lüscher's finite-volume prescription [41, 42]. For the low energy scattering of D and \bar{B}^* mesons, where other multi-particle thresholds are sufficiently high [61], in the S -wave leading to the total angular momentum and parity $J^P = 1^+$, the scattering phase shifts $\delta_{l=0}(k)$ are related to the finite-volume energy spectrum through $k \cot[\delta_0(k)] = 2Z_{00}[1; (\frac{kL}{2\pi})^2]/(L\sqrt{\pi})$. Here, $k(E_{cm} = \sqrt{s})$ is the momentum (energy) in the center of momentum frame such that $4sk^2 = (s - (M_D + M_{\bar{B}^*})^2)(s - (M_D - M_{\bar{B}^*})^2)$. We follow the procedure outlined in Appendix B of Ref. [62] to constrain the amplitude. A sub-threshold pole in the S -wave scattering amplitude $t = (\cot\delta_0 - i)^{-1}$ occurs when $k \cot\delta_0 = \pm\sqrt{-k^2}$ for scattering in S -wave.

We parametrize the elastic $D\bar{B}^*$ scattering amplitude in terms of the scattering length a_0 in an effective range expansion near the threshold, supplemented by a lattice spacing dependence. This is required to incorporate the cut-off effects observed in the ground state energy estimates. We find that a linear functional form given by $k \cot\delta_0 = A^{[0]} + aA^{[1]}$, where $A^{[0]} = -1/a_0$, accommodate the a dependence of the $k \cot\delta_0$ estimates. We present the fit results for $A^{[0]} = -1/a_0$ in Figure 4 (circle symbols) as a function of M_{ps} involved. Alternative fitting choices with a leading quadratic dependence or using only data from non-charm M_{ps} are consistent with results in Figure 4, see details in Supplemental material [58].

The sign of $A^{[0]} = -1/a_0$ determines the fate of the near-threshold pole, if there exists one. A negative (positive) value of $A^{[0]}(a_0)$ indicates that the interaction potential is strong enough to form a real bound state[63]. After considering all possible systematics, we find that for all the non-charm light quark masses, $A^{[0]}$ is negative, which indicates an attractive interaction strong enough to host a real bound state. On the contrary, at the charm point, despite the unambiguous negative energy shifts in the ground states, the attraction is weak to host any real bound state as suggested by the positive value of $k \cot\delta_0$ in the continuum limit. This observation goes in line with the phenomenological expectation for doubly heavy four quark ($QQ'l_1l_2$) systems with $m_{l_1} = m_{l_2}$ that the binding increases with increased relative heaviness of the heavy quarks with respect to its light quark content[14, 26, 64].

Now we investigate the light quark mass ($m_{u/d}$) or M_{ps} dependence of the fitted parameters. To this end, we consider three different parametrizations: a linear dependence ($f_l(M_{ps}) = \alpha_c + \alpha_l M_{ps}$) to probe the heavy light quark mass case, a leading M_{ps}^2 dependence ($f_s(M_{ps}) = \beta_c + \beta_s M_{ps}^2$) to assess the chiral behaviour, and a quadratic dependence ($f_q(M_{ps}) = \theta_c + \theta_l M_{ps} + \theta_s M_{ps}^2$) to quantify the associated systematics. In Figure 4, we show the fit results for this M_{ps} dependence in colored bands. The two stars represent $A^{[0]}$ at the physical M_{ps} (equivalently the physical scattering length a_0^{phys}) and the critical M_{ps} at which $A^{[0]}$ changes its sign or above which the system becomes unbound. It is indeed desired to have more

points in the intermediate mass regime between the charm and the strange quark masses to further constrain the

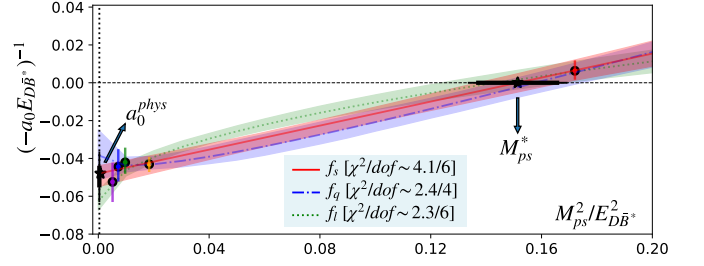


FIG. 4. Continuum extrapolated $k \cot\delta_0$ or $A^{[0]} = -1/a_0$ estimates of the $D\bar{B}^*$ system as a function of M_{ps}^2 in units of $E_{D\bar{B}^*}$. The dotted vertical line close to the y -axis indicates $M_{ps} = M_{\pi}^{phys}$. The two star symbols represent the amplitude at $M_{ps} = M_{\pi}^{phys}$ and the critical $M_{ps} = M_{ps}^*$ above which the system becomes unbound.

dependence. Yet, our fits demonstrate near independence in the fit forms as can be observed from the consistency between the error bands from different fit forms.

Based on the fit form $f_s(M_{ps})$ in the chiral regime, we find that the scattering length of the $D\bar{B}^*$ system at the physical light quark mass ($m_{u/d}^{phys}$), corresponding to $M_{ps} = M_{\pi}^{phys}$, to be

$$a_0^{phys} = 0.57(^{+4}_{-5})(17) \text{ fm}. \quad (3)$$

The asymmetric errors indicate the statistical uncertainties, whereas the second parenthesis quotes the systematic uncertainties with the most dominant contribution arising from the chiral extrapolation fit forms. The positive value of the scattering length at $M_{ps} = M_{\pi}^{phys}$, at the level of 3σ uncertainty, is an unambiguous evidence for the strength of the $D\bar{B}^*$ interaction potential to host a real $bc\bar{u}\bar{d}$ tetraquark bound state T_{bc} with binding energy

$$\delta m_{T_{bc}} = -43(^{+6}_{-7})(^{+14}_{-24}) \text{ MeV}, \quad (4)$$

with respect to $E_{D\bar{B}^*}$. The first parenthesis indicates the statistical errors and the second one quantifies various systematic uncertainties added in quadrature. The pseudoscalar meson mass, corresponding to the critical light quark mass, where a_0 diverges, is found to be $M_{ps}^* = 2.73(21)(19) \text{ GeV}$. This critical point also signifies that QCD dynamics within such exotic systems is such that at a heavy light quark mass the system of quarks perhaps reaches the unitary gas limit, as indicated by the divergent scattering length [65]. For $M_{ps} \geq M_{ps}^*$, the T_{bc} system remains unbound.

Systematic uncertainties: Our lattice setup together with the bare bottom and charm quark mass tuning procedure has been demonstrated to reproduce the $1S$ hyperfine splittings in quarkonia with uncertainties less than 6 MeV [50, 53]. We observe the effects of such a mistuning of either of the heavy quark mass on the energy splittings we

extract are very small compared to the statistical errors. Additionally, our strategy of evaluating the energy differences and working with mass ratios has also been shown to significantly mitigate the systematic uncertainties related to heavy quark masses [52, 53]. This is observed to be the case in this study as well, leading to transparent signals for the ground state energy as shown in Figures 1, 1, and 3. Our fitting procedure involves careful and conservative determination of statistical errors, and uncertainties related to the excited-state-contamination and fit-window errors. Additional checks using alternative quark smearing procedures also agree with our energy estimates, see Appendix A. The amplitude determination and followed extrapolations are performed with results from varying the fit-windows to evaluate the uncertainties propagated to our final results. The uncertainties related to the fit forms used in chiral extrapolations are observed to be the most dominant, as is evident from Figure 4. We assume the partially quenched setup involving ensembles with different sea pion masses, we utilize, have negligible effects on the energy splittings we extract for the explicitly exotic T_{bc} tetraquark, similar to what was observed for heavy hadrons in Refs. [66, 67]. Uncertainty related to scale setting is also found to be negligible in comparison to the statistical uncertainties in the energy splittings.

Summary: We have performed a lattice QCD simulation of coupled $D\bar{B}^*-\bar{B}D^*$ scattering with explicitly exotic flavor $bc\bar{u}\bar{d}$ and $I(J^P) = 0(1^+)$. Following a rigorous extraction of finite-volume eigenenergies and continuum extrapolated elastic $D\bar{B}^*$ scattering amplitudes for the five light quark masses studied, we determine the light quark mass dependence of the elastic $D\bar{B}^*$ scattering length a_0 . We observe unambiguous negative energy shifts between the interacting and non-interacting finite-volume energy levels. Our estimate for a_0^{phys} (Eq. (3)) is positive, indicating an attractive interaction between the D and \bar{B}^* mesons, which is strong enough to host a real bound state with binding energy $\delta m_{T_{bc}} = -43(^{+6}_{-7})(^{+14}_{-24})$ MeV. We find that the strength of interaction is such that this $bc\bar{u}\bar{d}$ tetraquark becomes unbound at M_{ps}^* , which is close to the η_c meson mass.

In this work, we make several important steps ahead to arrive at robust inference on the nature of interaction between the D and \bar{B}^* mesons. Our main strategy has been to determine the signature of scattering length in $D\bar{B}^*$ interactions at the physical pion mass a_0^{phys} . Our results indicate that a_0^{phys} is positive, which suggests that attractive $D\bar{B}^*$ interactions are strong enough to host a real bound state. Further theoretical investigations are desired to reduce the uncertainties in the binding energy of T_{bc} with respect to $E_{D\bar{B}^*}$. Fully dynamical simulations on several more ensembles, with different volumes and improved fermion actions, high statistics studies with lighter $m_{u/d}$, etc. are a few other improvisations that can further constrain the relevant scattering amplitude. Additionally, future works involving Hermitian correlation

matrices at rest as well as in moving frames and those using bilocal two-meson interpolators with nonzero relative meson momenta aimed at reliable excited state extraction would be a few important steps ahead [55, 62, 68, 69]. We hope that our observations and inferences in this work will motivate more theoretical efforts and experimental searches for such states.

This work is supported by the Department of Atomic Energy, Government of India, under Project Identification Number RTI 4002. M.P. gratefully acknowledges support from the Department of Science and Technology, India, SERB Start-up Research Grant No. SRG/2023/001235. We are thankful to the MILC collaboration and in particular to S. Gottlieb for providing us with the HISQ lattice ensembles. We thank Sara Collins for a careful reading of the manuscript. We thank the authors of Ref. [70] for making the *TwoHadronsInBox* package utilized in this work. We also thank Gunnar Bali, Parikshit Junnarkar, Alexey Nefediev, Sayantan Sharma, Stephen R. Sharpe, and Tanishk Shrimal for discussions. Computations were carried out on the Cray-XC30 of ILGTI, TIFR. Amplitude analyses were performed on Nandadevi computing cluster at IISc Chennai. N. M. would also like to thank A. Salve and K. Ghadiali for computational support.

Appendix A: Ground state energy plateau.— In this work we have utilized a wall-source point-sink setup to construct the necessary two-point correlation functions. The use of such an asymmetric setup implies the effective energies $aE_{eff} = [\ln(C(t)/C(t+\delta t))]/\delta t$ could approach their asymptotic values as rising-from-below, due to the nonpositive definite nature of the coefficients in a spectral decomposition, in contrast to a falling-from-above behaviour in a symmetric setup. In Figure 5, we show the effective mass in wall-source point-sink setup with the brown-circle ($R^2 = 0$) which rises from below.

To avoid any ambiguity in selecting the plateau regions of effective masses of such correlators, we also employ a wall-source box-sink setup [29], which asymptotically approaches the symmetric limit. In the symmetric limit, the effective masses are expected to follow a conventional falling-from-above feature, modulo the statistical noise. To this end, we vary the smearing radius R to investigate the time dependence of effective mass plateaus in the approach to the symmetric limit. In Figure 5, we present a comparison of the effective energy (top) and effective energy splittings (bottom) determined using different quark sink smearing procedures for the case of $M_{ps} \sim 700$ MeV on the finest ensemble. Clearly the rising-from-below behaviour is gradually disappearing in the approach to the symmetric limit. It is also evident that the results at the large time limit from point-sink and box-sink are very much consistent with each other affirming our assessment on effective mass plateau in choosing a fit range. Such a behavior of effective masses with varying smearing radii was also observed in Ref. [29]. In the large time limit, where the signal quality is still good, all of sink smearing

cases suggest consistent negative energy shifts. This is evident from the large time behaviour of energy splittings presented in the bottom panel of Figure 5, where the correlated statistical noise, not related to the excited state contamination, is suppressed between the numerator and denominator in the ratio correlators $R^n(t)$.

The agreement of energy splitting estimates from fits to $R^n(t)$ with those evaluated from separate fits to the GEVP eigenvalue correlators $\lambda^n(t)$ and the single-meson correlators $\mathcal{C}_{D/\bar{B}^*}$ at large times (see Figure 1) already rules out the usual concern of accidental partial cancellation of excited state contaminations in $R^n(t)$. The consistency at large times between ground state energy plateaus from different sink-smearing radii observed in top panel of Figure 5 further affirms the reliable isolation of the ground state plateau. Note also that the magnitude of such cancellations and the ground state saturation times could be different in different lattice QCD ensembles. All the ground state estimates for noncharm M_{ps} values in our study are determined from the time intervals approximately between 1.5(2) fm [t_{min}] to 2.3(2) fm [t_{max}]. The consistent ground state saturation times across different ensembles with different specifications further imply the reliability of our ground state saturation, despite our asymmetric setup.

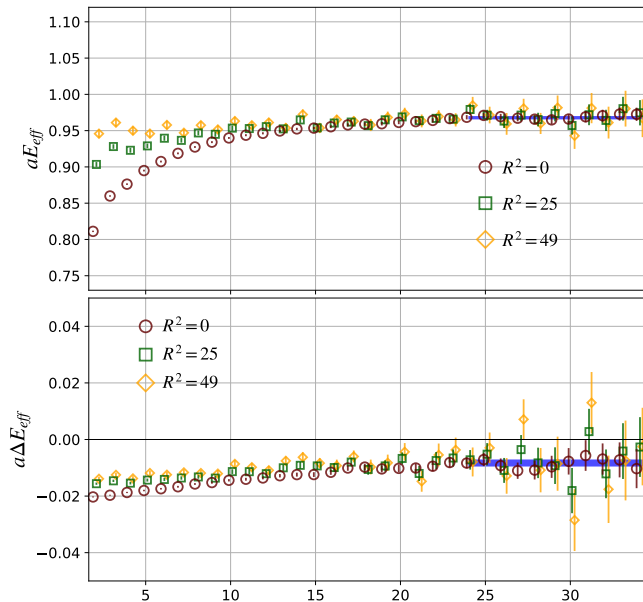


FIG. 5. Comparison of effective energy (top) and effective energy splitting (bottom) for the ground state as determined using three different smearing radii applied on the quark fields at the sink timeslice. The legend indicates the smearing radius squared in units of the lattice spacing [29]. The blue horizontal band indicates the final fit estimate for the energy and energy splitting. The results presented are for the case $M_{ps} \sim 700$ MeV on the finest ensemble.

Appendix B: Elastic $D\bar{B}^$ excitations.*— Gaining access to higher lying elastic excitations in the $D\bar{B}^*$ channel is

an important step ahead towards constraining the energy dependence of the amplitude over a long energy range. However, within the wall-smearing setup, all the nonzero momentum excitations are significantly suppressed. This suppression is exact in a free theory, and is empirically confirmed from the early plateauing and from the quality of signals in the interacting theory. While this suppression is advantageous in ground state energy determination (see Refs.[14, 16, 28, 29, 52, 53] for details), the suppressed coupling to the nonzero momentum excitations implies that the access to higher two-meson elastic excitations with nonzero relative meson momenta are restricted in the wall-smearing setup. This implies other methodologies that facilitate the use of bilocal two-meson interpolators with separately momentum projected mesons are necessary in future studies [55, 71, 72]³. In this respect, it is informative to know the location of the lowest non-interacting level with nonzero relative meson momenta and whether it is close enough to influence the ground state energies in any substantial way. Considering this, in Figure 6 we present the ground state eigenenergies along with the $D\bar{B}^*$ threshold and the next lowest elastic $D\bar{B}^*$ excitation with nonzero relative meson momentum determined using the continuum dispersion relation that is assumed in the finite-volume quantization condition [41, 42]. Clearly, the location of this first non-interacting elastic excitation is sufficiently high to have any nonnegligible effects on the extracted the ground state energies.

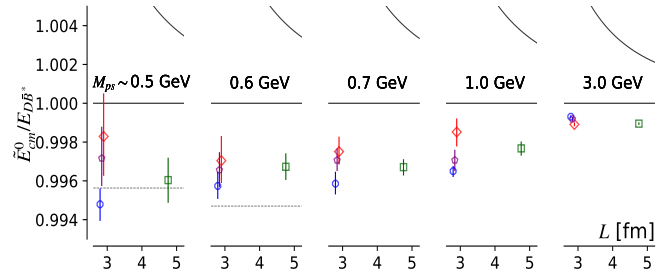


FIG. 6. The ground state energy eigenvalues in the background of lowest two non-interacting $D\bar{B}^*$ finite-volume levels units of $E_{D\bar{B}^*}$ on all ensembles (see Table I for color-symbol conventions) for all M_{ps} values (different vertical panels).

* padmanath@imsc.res.in
† archana.radhakrishnan@tifr.res.in
‡ nilmani@theory.tifr.res.in

[1] R. Aaij *et al.* (LHCb), Observation of an exotic narrow doubly charmed tetraquark, *Nature Phys.* **18**, 751 (2022).

³ While this letter was being reviewed, a preprint, Ref. [73] appeared which utilizes bilocal two-meson interpolators in their analysis, utilizing the methods in Ref. [72].

- [2] J. P. Ader, J. M. Richard, and P. Taxil, Do narrow heavy multi - quark states exist?, *Phys. Rev. D* **25**, 2370 (1982).
- [3] J. I. Ballot and J. M. Richard, Four quark states in additive potentials, *Phys. Lett. B* **123**, 449 (1983).
- [4] S. Zouzou, B. Silvestre-Brac, C. Gignoux, and J. M. Richard, Four quark bound states, *Z. Phys. C* **30**, 457 (1986).
- [5] L. Heller and J. A. Tjon, On the Existence of Stable Dimesons, *Phys. Rev. D* **35**, 969 (1987).
- [6] J. Carlson, L. Heller, and J. A. Tjon, Stability of Dimesons, *Phys. Rev. D* **37**, 744 (1988).
- [7] A. V. Manohar and M. B. Wise, Exotic Q Q anti-q anti-q states in QCD, *Nucl. Phys. B* **399**, 17 (1993).
- [8] D. Janc and M. Rosina, The $T_{cc} = DD^*$ molecular state, *Few Body Syst.* **35**, 175 (2004).
- [9] D. Ebert, R. N. Faustov, V. O. Galkin, and W. Lucha, Masses of tetraquarks with two heavy quarks in the relativistic quark model, *Phys. Rev. D* **76**, 114015 (2007).
- [10] F. S. Navarra, M. Nielsen, and S. H. Lee, QCD sum rules study of QQ - anti-u anti-d mesons, *Phys. Lett. B* **649**, 166 (2007).
- [11] E. J. Eichten and C. Quigg, Heavy-quark symmetry implies stable heavy tetraquark mesons $Q_i Q_j \bar{q}_k \bar{q}_l$, *Phys. Rev. Lett.* **119**, 202002 (2017).
- [12] M. Karliner and J. L. Rosner, Discovery of doubly-charmed Ξ_{cc} baryon implies a stable $(bb\bar{u}\bar{d})$ tetraquark, *Phys. Rev. Lett.* **119**, 202001 (2017).
- [13] P. Bicudo, K. Cichy, A. Peters, and M. Wagner, BB interactions with static bottom quarks from Lattice QCD, *Phys. Rev. D* **93**, 034501 (2016).
- [14] A. Francis, R. J. Hudspith, R. Lewis, and K. Maltman, Lattice Prediction for Deeply Bound Doubly Heavy Tetraquarks, *Phys. Rev. Lett.* **118**, 142001 (2017).
- [15] P. Bicudo, M. Cardoso, A. Peters, M. Pflaumer, and M. Wagner, $ud\bar{b}\bar{b}$ tetraquark resonances with lattice QCD potentials and the Born-Oppenheimer approximation, *Phys. Rev. D* **96**, 054510 (2017).
- [16] P. Junnarkar, N. Mathur, and M. Padmanath, Study of doubly heavy tetraquarks in Lattice QCD, *Phys. Rev. D* **99**, 034507 (2019).
- [17] L. Leskovec, S. Meinel, M. Pflaumer, and M. Wagner, Lattice QCD investigation of a doubly-bottom $\bar{b}b\bar{u}\bar{d}$ tetraquark with quantum numbers $I(J^P) = 0(1^+)$, *Phys. Rev. D* **100**, 014503 (2019).
- [18] R. J. Hudspith and D. Mohler, Exotic tetraquark states with two b^- quarks and $JP=0+$ and $1+$ Bs states in a nonperturbatively tuned lattice NRQCD setup, *Phys. Rev. D* **107**, 114510 (2023).
- [19] R. Aaij *et al.* (LHCb), Observation of the doubly charmed baryon Ξ_{cc}^{++} , *Phys. Rev. Lett.* **119**, 112001 (2017).
- [20] A. Tumasyan *et al.* (CMS), Observation of triple J/ψ meson production in proton-proton collisions, *Nature Phys.* **19**, 338 (2023), [Erratum: *Nature Phys.* **19**, (2023)].
- [21] R. Aaij *et al.* (LHCb), Associated production of prompt J/ψ and Υ mesons in pp collisions at $\sqrt{s} = 13$ TeV, (2023).
- [22] V. Khachatryan *et al.* (CMS), Observation of $\Upsilon(1S)$ pair production in proton-proton collisions at $\sqrt{s} = 8$ TeV, *JHEP* **05**, 013.
- [23] T. Gershon and A. Poluektov, Displaced B_c^- mesons as an inclusive signature of weakly decaying double beauty hadrons, *JHEP* **01**, 019.
- [24] Q. Qin, Y.-J. Shi, W. Wang, G.-H. Yang, F.-S. Yu, and R. Zhu, Inclusive approach to hunt for the beauty-charmed baryons Ξ_{bc} , *Phys. Rev. D* **105**, L031902 (2022).
- [25] I. Polyakov, Doubly charmed tetraquarks T_{cc} and new road it opens, in *20th International Conference on Hadron Spectroscopy and Structure* (2023).
- [26] A. Czarnecki, B. Leng, and M. B. Voloshin, Stability of tetrons, *Phys. Lett. B* **778**, 233 (2018).
- [27] S. S. Agaev, K. Azizi, and H. Sundu, Hadronic molecule model for the doubly charmed state T_{cc}^+ , *JHEP* **06**, 057.
- [28] A. Francis, R. J. Hudspith, R. Lewis, and K. Maltman, Evidence for charm-bottom tetraquarks and the mass dependence of heavy-light tetraquark states from lattice QCD, *Phys. Rev. D* **99**, 054505 (2019).
- [29] R. J. Hudspith, B. Colquhoun, A. Francis, R. Lewis, and K. Maltman, A lattice investigation of exotic tetraquark channels, *Phys. Rev. D* **102**, 114506 (2020).
- [30] S. Meinel, M. Pflaumer, and M. Wagner, Search for $b^-b^-u\bar{s}$ and $b^-c^-u\bar{d}$ tetraquark bound states using lattice QCD, *Phys. Rev. D* **106**, 034507 (2022).
- [31] W. Chen, T. G. Steele, and S.-L. Zhu, Exotic open-flavor $bc\bar{q}\bar{q}$, $bc\bar{s}\bar{s}$ and $qc\bar{q}\bar{b}$, $sc\bar{s}\bar{b}$ tetraquark states, *Phys. Rev. D* **89**, 054037 (2014).
- [32] S. Sakai, L. Roca, and E. Oset, Charm-beauty meson bound states from $B(B^*)D(D^*)$ and $B(B^*)\bar{D}(\bar{D}^*)$ interaction, *Phys. Rev. D* **96**, 054023 (2017).
- [33] T. F. Caramés, J. Vijande, and A. Valcarce, Exotic $bc\bar{q}\bar{q}$ four-quark states, *Phys. Rev. D* **99**, 014006 (2019).
- [34] W. Park, S. Noh, and S. H. Lee, Masses of the doubly heavy tetraquarks in a constituent quark model, *Nucl. Phys. A* **983**, 1 (2019).
- [35] C. Deng, H. Chen, and J. Ping, Systematical investigation on the stability of doubly heavy tetraquark states, *Eur. Phys. J. A* **56**, 9 (2020).
- [36] G. Yang, J. Ping, and J. Segovia, Doubly-heavy tetraquarks, *Phys. Rev. D* **101**, 014001 (2020).
- [37] S. S. Agaev, K. Azizi, and H. Sundu, Double-heavy axial-vector tetraquark $T_{bc;\bar{u}\bar{d}}^0$, *Nucl. Phys. B* **951**, 114890 (2020).
- [38] Q.-F. Lü, D.-Y. Chen, and Y.-B. Dong, Masses of doubly heavy tetraquarks $T_{QQ'}$ in a relativized quark model, *Phys. Rev. D* **102**, 034012 (2020).
- [39] Y. Tan, W. Lu, and J. Ping, Systematics of $QQ\bar{q}\bar{q}$ in a chiral constituent quark model, *Eur. Phys. J. Plus* **135**, 716 (2020).
- [40] E. Braaten, L.-P. He, and A. Mohapatra, Masses of doubly heavy tetraquarks with error bars, *Phys. Rev. D* **103**, 016001 (2021).
- [41] M. Luscher, Two particle states on a torus and their relation to the scattering matrix, *Nucl. Phys. B* **354**, 531 (1991).
- [42] R. A. Briceno, Two-particle multichannel systems in a finite volume with arbitrary spin, *Phys. Rev. D* **89**, 074507 (2014).
- [43] A. Bazavov *et al.* (MILC), Lattice QCD Ensembles with Four Flavors of Highly Improved Staggered Quarks, *Phys. Rev. D* **87**, 054505 (2013).
- [44] Y. Chen, S. J. Dong, T. Draper, I. Horvath, F. X. Lee, K. F. Liu, N. Mathur, and J. B. Zhang, Chiral logarithms in quenched QCD, *Phys. Rev. D* **70**, 034502 (2004).
- [45] A. Li *et al.* (xQCD), Overlap Valence on 2+1 Flavor Domain Wall Fermion Configurations with Deflation and Low-mode Substitution, *Phys. Rev. D* **82**, 114501 (2010).
- [46] G. P. Lepage, L. Magnea, C. Nakhleh, U. Magnea, and K. Hornbostel, Improved nonrelativistic QCD for heavy

- quark physics, *Phys. Rev.* **D46**, 4052 (1992).
- [47] A. X. El-Khadra, A. S. Kronfeld, and P. B. Mackenzie, Massive fermions in lattice gauge theory, *Phys. Rev. D* **55**, 3933 (1997).
- [48] S. Basak, S. Datta, M. Padmanath, P. Majumdar, and N. Mathur, Charm and strange hadron spectra from overlap fermions on HISQ gauge configurations, *Proceedings, 30th International Symposium on Lattice Field Theory (Lattice 2012): Cairns, Australia, June 24-29, 2012*, PoS **LATTICE2012**, 141 (2012).
- [49] S. Basak, S. Datta, A. T. Lytle, M. Padmanath, P. Majumdar, and N. Mathur, Hadron spectra from overlap fermions on HISQ gauge configurations, *Proceedings, 31st International Symposium on Lattice Field Theory (Lattice 2013): Mainz, Germany, July 29-August 3, 2013*, PoS **LATTICE2013**, 243 (2014).
- [50] N. Mathur, M. Padmanath, and R. Lewis, Charmed-Bottom Mesons from Lattice QCD, *Proceedings, 34th International Symposium on Lattice Field Theory (Lattice 2016): Southampton, UK, July 24-30, 2016*, PoS **LATTICE2016**, 100 (2016).
- [51] B. Chakraborty, C. T. H. Davies, B. Galloway, P. Knecht, J. Koponen, G. C. Donald, R. J. Dowdall, G. P. Lepage, and C. McNeile, High-precision quark masses and QCD coupling from $n_f = 4$ lattice QCD, *Phys. Rev. D* **91**, 054508 (2015).
- [52] N. Mathur, M. Padmanath, and S. Mondal, Precise predictions of charmed-bottom hadrons from lattice QCD, *Phys. Rev. Lett.* **121**, 202002 (2018).
- [53] N. Mathur, M. Padmanath, and D. Chakraborty, Strongly Bound Dibaryon with Maximal Beauty Flavor from Lattice QCD, *Phys. Rev. Lett.* **130**, 111901 (2023).
- [54] M. Padmanath, C. B. Lang, and S. Prelovsek, $X(3872)$ and $Y(4140)$ using diquark-antidiquark operators with lattice QCD, *Phys. Rev.* **D92**, 034501 (2015).
- [55] M. Wagner, C. Alexandrou, J. Finkenrath, T. Leontiou, S. Meinel, and M. Pflaumer, Lattice QCD study of antiheavy-antiheavy-light-light tetraquarks based on correlation functions with scattering interpolating operators both at the source and at the sink, *PoS LATTICE2022*, 270 (2023).
- [56] C. Michael, Adjoint Sources in Lattice Gauge Theory, *Nucl. Phys.* **B259**, 58 (1985).
- [57] J. R. Green, A. D. Hanlon, P. M. Junnarkar, and H. Wittig, Weakly Bound H Dibaryon from $SU(3)$ -Flavor-Symmetric QCD, *Phys. Rev. Lett.* **127**, 242003 (2021).
- [58] *Supplemental material: We present various technical details of the work: Finite-volume eigenenergies on all lattice QCD ensembles, amplitude fits, and quark mass dependence fits are shown here. Additional publications cited in this material are [54, 74, 75].*
- [59] *We also observe statistically significant negative energy shifts of similar magnitude for the ground states in $D\bar{B}$ two-meson energy spectrum at different light quark masses with isoscalar scalar $[I(J^P) = 0(0^+)]$ quantum numbers and explicitly exotic flavor content $bc\bar{u}\bar{d}$. This work is reported in Ref. [76].*
- [60] M.-L. Du, A. Filin, V. Baru, X.-K. Dong, E. Epelbaum, F.-K. Guo, C. Hanhart, A. Nefediev, J. Nieves, and Q. Wang, Role of left-hand cut contributions on pole extractions from lattice data: Case study for $T_{cc}(3875)^+$, (2023).
- [61] Z. T. Draper and S. R. Sharpe, Applicability of the two-particle quantization condition to partially-quenched theories, *Phys. Rev. D* **104**, 034510 (2021).
- [62] M. Padmanath and S. Prelovsek, Signature of a Doubly Charm Tetraquark Pole in DD^* Scattering on the Lattice, *Phys. Rev. Lett.* **129**, 032002 (2022).
- [63] L. D. Landau and E. M. Lifshitz, *Quantum Mechanics: Non-Relativistic Theory*, Course of Theoretical Physics, Vol. v.3 (Butterworth-Heinemann, Oxford, 1991).
- [64] P. Junnarkar, M. Padmanath, and N. Mathur, Heavy light tetraquarks from Lattice QCD, *Proceedings, 35th International Symposium on Lattice Field Theory (Lattice 2017): Granada, Spain, June 18-24, 2017*, *EPJ Web Conf.* **175**, 05014 (2018).
- [65] R. G. Newton, *Scattering Theory of Waves and Particles* (2013).
- [66] R. J. Dowdall, C. T. H. Davies, T. C. Hammant, and R. R. Horgan, Precise heavy-light meson masses and hyperfine splittings from lattice QCD including charm quarks in the sea, *Phys. Rev.* **D86**, 094510 (2012).
- [67] C. McNeile, C. T. H. Davies, E. Follana, K. Hornbostel, and G. P. Lepage, Heavy meson masses and decay constants from relativistic heavy quarks in full lattice QCD, *Phys. Rev.* **D86**, 074503 (2012).
- [68] M. Padmanath, S. Collins, D. Mohler, S. Piemonte, S. Prelovsek, A. Schäfer, and S. Weishaupl, Identifying spin and parity of charmonia in flight with lattice QCD, *Phys. Rev. D* **99**, 014513 (2019).
- [69] S. Chen, C. Shi, Y. Chen, M. Gong, Z. Liu, W. Sun, and R. Zhang, $T_{cc}^+(3875)$ relevant DD^* scattering from $N_f=2$ lattice QCD, *Phys. Lett. B* **833**, 137391 (2022).
- [70] C. Morningstar, J. Bulava, B. Singha, R. Brett, J. Fallica, A. Hanlon, and B. Hörz, Estimating the two-particle K -matrix for multiple partial waves and decay channels from finite-volume energies, *Nucl. Phys. B* **924**, 477 (2017).
- [71] M. Peardon, J. Bulava, J. Foley, C. Morningstar, J. Dudek, R. G. Edwards, B. Joo, H.-W. Lin, D. G. Richards, and K. J. Juge (Hadron Spectrum), A Novel quark-field creation operator construction for hadronic physics in lattice QCD, *Phys. Rev. D* **80**, 054506 (2009).
- [72] A. Abdel-Rehim, C. Alexandrou, J. Berlin, M. Dalla Brida, J. Finkenrath, and M. Wagner, Investigating efficient methods for computing four-quark correlation functions, *Comput. Phys. Commun.* **220**, 97 (2017).
- [73] C. Alexandrou, J. Finkenrath, T. Leontiou, S. Meinel, M. Pflaumer, and M. Wagner, Shallow Bound States and Hints for Broad Resonances with Quark Content $b\bar{c}u\bar{d}$ in $B\bar{D}^-$ and $B^*\bar{D}^-$ Scattering from Lattice QCD, *Phys. Rev. Lett.* **132**, 151902 (2024).
- [74] J. J. Dudek, R. G. Edwards, M. J. Peardon, D. G. Richards, and C. E. Thomas, Highly excited and exotic meson spectrum from dynamical lattice QCD, *Phys. Rev. Lett.* **103**, 262001 (2009).
- [75] M. Padmanath, R. G. Edwards, N. Mathur, and M. Peardon, Spectroscopy of triply-charmed baryons from lattice QCD, *Phys. Rev.* **D90**, 074504 (2014).
- [76] A. Radhakrishnan, M. Padmanath, and N. Mathur, Study of isoscalar scalar $bc\bar{u}\bar{d}$ tetraquark T_{bc} from lattice QCD, (2024).

Supplemental material

I. LOW LYING EIGENENERGIES ON ALL ENSEMBLES

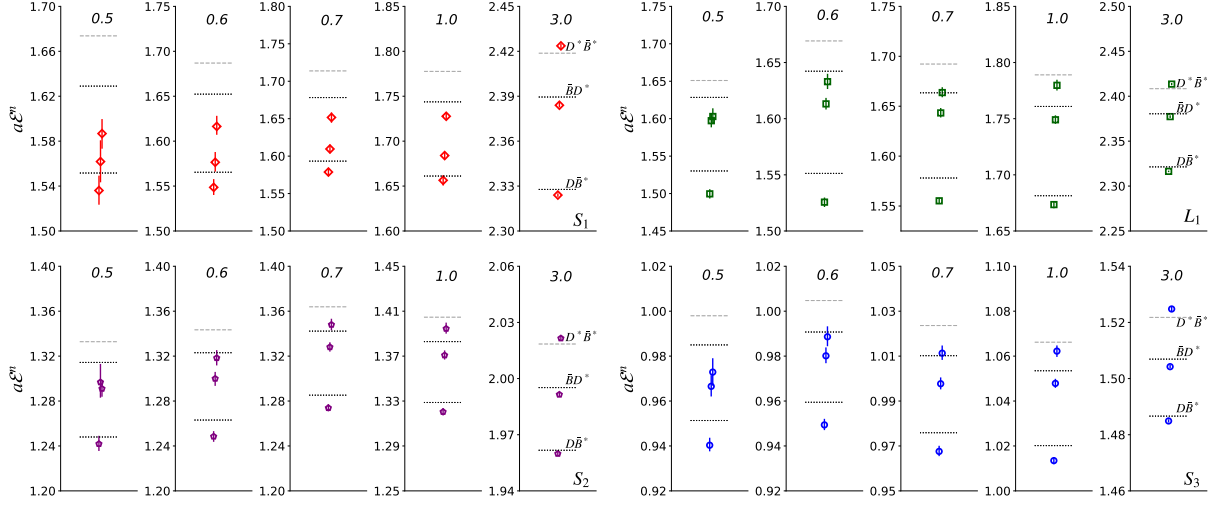


FIG. 1. Low-lying finite-volume eigenenergies for isoscalar axialvector $bc\bar{u}\bar{d}$ channel on the four ensembles studied. The near degenerate eigenlevels are slightly shifted horizontally for clarity.

In this section, we present the finite-volume GEVP eigenenergies of the isoscalar axialvector $bc\bar{u}\bar{d}$ channel that we extract on all four ensembles listed in Table I of the main article, at the five different $m_{u/d}$ values corresponding to $M_{ps} \sim 0.5, 0.6, 0.7, 1.0$, and 3.0 GeV. The eigenenergies shown in lattice units include the additive offsets related to the NRQCD-based dynamics of heavy bottom quarks. The non-interacting two-meson energy levels corresponding to $D\bar{B}^*$ and $\bar{B}D^*$ thresholds are indicated as dotted horizontal line segments for each lattice and each M_{ps} . The $D^*\bar{B}^*$ threshold in each case is also shown in the figure by dashed lines. Note that the use of wall-smearing setup restricts any direct access to the elastic two-meson excitations with nonzero relative meson momenta. This means although a reliable ground state extraction could be made, the excited eigenenergies may not represent the real elastic excitations.

II. OPERATOR-STATE OVERLAPS

In Figure 2, we present the modulus of normalized sink operator-state overlaps $|\tilde{Z}_i^n|$, normalized such that its largest value for any given operator \mathcal{O}_i across all the eigenenergies $\{n\}$ is unity [74, 75]. \tilde{Z}_i^n quantifies the relative relevance of any given operator across all the eigenenergies. The $|\tilde{Z}_i^n|$ values are presented for all M_{ps} cases on the L_1 ensemble. Each square marker corresponds to the $|\tilde{Z}_i^n|$ for a given operator \mathcal{O}_i on to a given eigenenergy n . Each horizontal panel stands for an M_{ps} indicated on the right-hand side, whereas the vertical lines in each horizontal panel part $|\tilde{Z}_i^n|$ for different operators indicated on the top panel. The x -axis ticks refer to the three finite-volume eigenenergies we have extracted. \mathcal{O}_1 , the two-meson operator related to $D\bar{B}^*$ threshold, can be seen to have the largest overlap with the ground state and has significantly small overlaps with the excited eigenenergies. \mathcal{O}_2 , the two-meson operator related to $\bar{B}D^*$ threshold, has the largest overlap with the first excited eigenenergy and a very small overlap with the ground state. \mathcal{O}_2 also have nonnegligible overlap factors with the second excited eigenenergy indicating $\bar{B}D^*$ -type two-meson Fock component, which decreases with increasing M_{ps} . On the other hand, \mathcal{O}_3 , the diquark-antidiquark type operator, have substantial overlap factors with all eigenenergies at the two lightest M_{ps} values, whereas with an increased M_{ps} its largest overlap is with the second excited eigenenergy. Note that \mathcal{O}_3 is Fierz related to two-meson interpolators [54], and the large \tilde{Z}_3^n values of \mathcal{O}_3 for all n could be related to this underlying connection between two-meson and diquark-antidiquark operators.

A summary from the above observations on overlap factors is as follows. \mathcal{O}_1 predominantly determines the ground state, whereas it has significantly small coupling with the excited eigenenergies. Similar patterns of overlap factors are also observed for other ensembles, all of which indicate that \mathcal{O}_1 predominantly determines the ground state. The two excited eigenenergies have strong two-meson and diquark-antidiquark Fock components in the two lightest M_{ps} values.

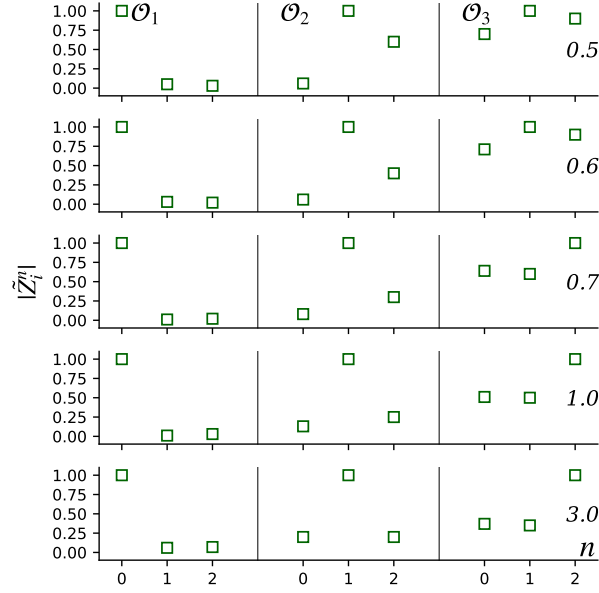


FIG. 2. Modulus of normalized sink operator-state overlaps $|\tilde{Z}_t^n|$ for an eigenenergy indicated by $n = 0, 1, 2$ and an operator represented by \mathcal{O}_i , where $i = 1, 2, 3$ on the L_1 ensemble. The errors in the normalized overlap factors are smaller than the symbols and hence are suppressed.

One could also evaluate and investigate the normalized source operator-state overlaps from the left eigenvectors of \mathcal{C} in Eq. (1) in the main draft, which also leads to the same conclusions.

III. OPERATOR BASIS DEPENDENCE

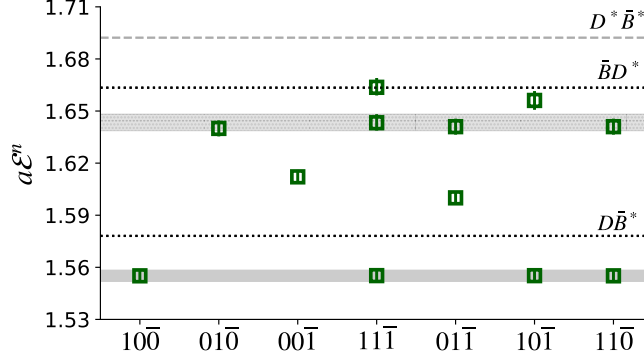


FIG. 3. Operator basis dependence of the low lying eigenenergies of the L_1 ensemble and $M_{ps} \sim 700$ MeV for all possible operator basis that can be built out of the three operators utilized in this work.

In Figure 3, we show the operator basis dependence as determined for $M_{ps} \sim 700$ MeV in the L_1 ensemble, for various operator basis build out of \mathcal{O}_1 , \mathcal{O}_2 , and \mathcal{O}_3 operators as defined in Eq. (2) of the main draft. The digital indexing on the x -axis tick labels refers to various operator basis in the order $\{\mathcal{O}_1, \mathcal{O}_2, \mathcal{O}_3\}$, with an overline on the third index as a visual aid within the plot to highlight the diquark-antidiquark interpolator. 1 (0) indicates an operator is included in (excluded from) the basis. The horizontal lines refer to the $D\bar{B}^*$, $\bar{B}D^*$ and \bar{B}^*D thresholds. The gray horizontal bands refer to the two lowest levels in the full basis indicated by $11\bar{1}$. A level below the threshold appears only when \mathcal{O}_1 is present in the basis. The first excited eigenenergy in the full basis $11\bar{1}$ is faithfully reproduced in those bases where \mathcal{O}_2 is included. \mathcal{O}_3 alone does not precisely determine any level among the GEVP eigenenergies using full basis. Similar observations are also made on other ensembles. In summary, the ground state in the full basis

$11\bar{1}$ is reliably determined with \mathcal{O}_1 and is unaffected by the inclusion of \mathcal{O}_2 and \mathcal{O}_3 operators.

M_{ps} [GeV]	$\chi^2/d.o.f$	Linear		$\chi^2/d.o.f$	Quadratic	
		$A^{[0]}/E_{D\bar{B}^*}$	$A^{[1]}/E_{D\bar{B}^*}$		$A^{[0]}/E_{D\bar{B}^*}$	$A^{[2]}/E_{D\bar{B}^*}$
0.5	2.1/2	-0.05(1)	0.17($^{+13}_{-11}$)	2.1/2	-0.045(6)	0.9($^{+7}_{-6}$)
0.6	0.5/2	-0.044($^{+9}_{-8}$)	0.10($^{+9}_{-9}$)	0.5/2	-0.040($^{+6}_{-5}$)	0.6(5)
0.7	3.0/2	-0.042($^{+8}_{-6}$)	0.09($^{+6}_{-7}$)	3.7/2	-0.037($^{+5}_{-4}$)	0.5($^{+3}_{-4}$)
1.0	2.9/2	-0.043(4)	0.11($^{+5}_{-5}$)	2.9/2	-0.038($^{+3}_{-3}$)	0.8(3)
3.0	3.6/2	0.006($^{+6}_{-5}$)	-0.20($^{+4}_{-5}$)	3.6/2	-0.002($^{+4}_{-3}$)	-1.2($^{+2}_{-3}$)

TABLE I. Results from amplitude fits at different light quark mass cases indicated in terms of M_{ps} in the first column. The amplitude is approximated to be determined by the scattering length, with a linear or quadratic lattice spacing dependence as discussed in the main draft. The optimized parameter values in the table are presented in units of energy of the $D\bar{B}^*$ threshold, $E_{D\bar{B}^*}$. The $A^{[0]}$ parameter in either parametrization is negative of the inverse scattering length in the continuum limit.

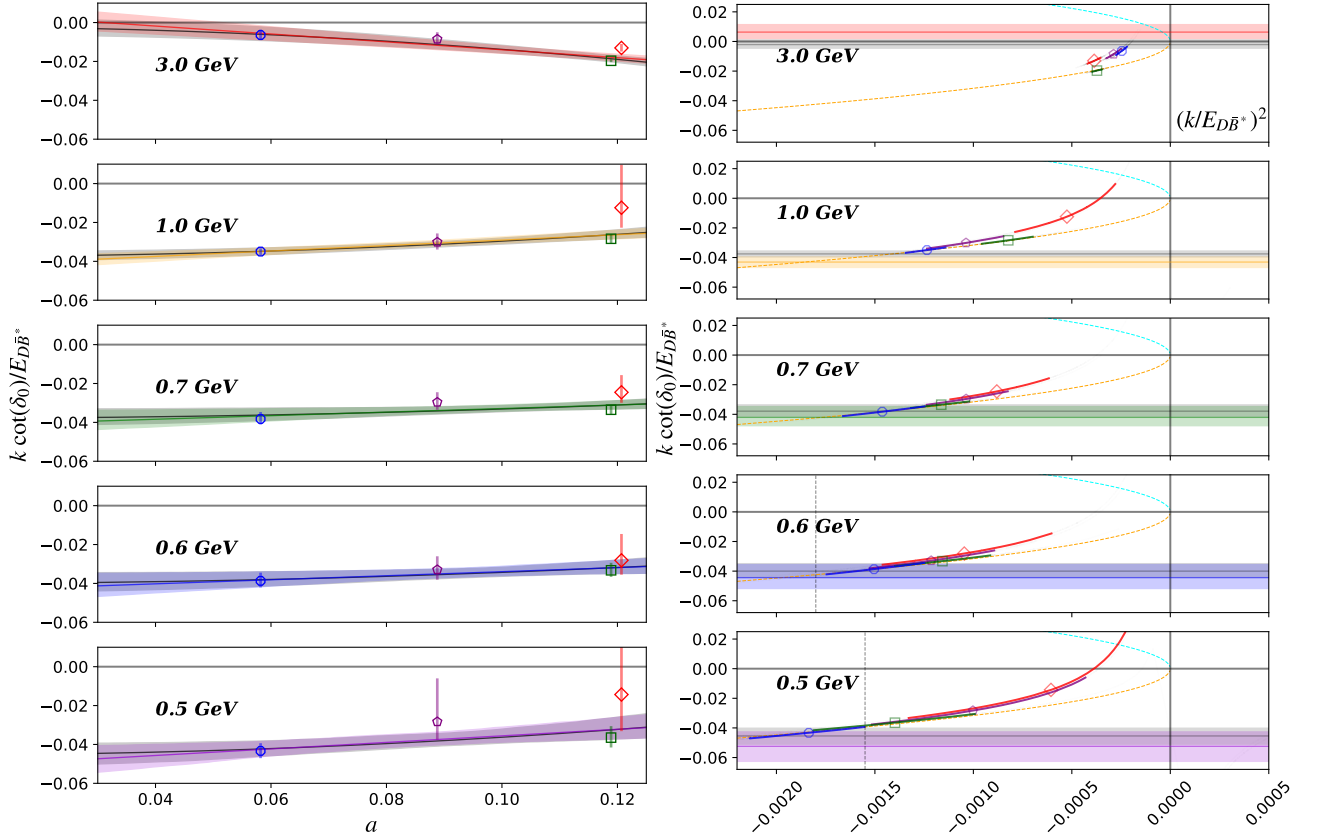


FIG. 4. Left: $k \cot \delta_0$, in units of the elastic threshold $E_{D\bar{B}^*}$, versus a (lattice spacing) for all M_{ps} values. We follow the marker/color coding in Table I of the main draft for the data points referring to the simulated data. The colored/gray bands indicate the fit results with linear and quadratic lattice spacing dependence, respectively. Right: $k \cot \delta_0$ versus k^2 for all M_{ps} values studied in units of the elastic threshold $E_{D\bar{B}^*}$. The dashed orange (cyan) curve indicates the constraint for the existence of a sub-threshold pole in the scattering amplitude. The horizontal bands are the continuum extrapolated estimates of $k \cot \delta_0$ for the respective M_{ps} . The black dashed vertical lines in the plots on the right indicate the location of the branch point associated with the left hand cut arising from the $D\bar{B}\pi$ channel.

IV. RESULTS ON SCATTERING AMPLITUDE

In Table I, we tabulate the results from different amplitude fits that were performed. In Figure 4, we present the quality of these fits by comparing the fit results with the data points (see the figure caption for details). On the left of

Figure 5, we present the light quark mass dependence in the chiral regime determined from continuum extrapolated elastic DB^* scattering amplitudes following a linear and quadratic lattice spacing dependence. We present the final estimate (black star) from the linear fit form considering the presence of heavy quarks in our system, whereas the difference in the fit results are accounted in the systematics quoted in the main draft. On the right of Figure 5, we present a comparison of the light quark mass dependence in the chiral regime between the fit involving all M_{ps} datasets and the fit involving the lightest four M_{ps} datasets. Either fitting procedures can be seen to be consistent with our final estimate in the chiral limit is shown by black star.

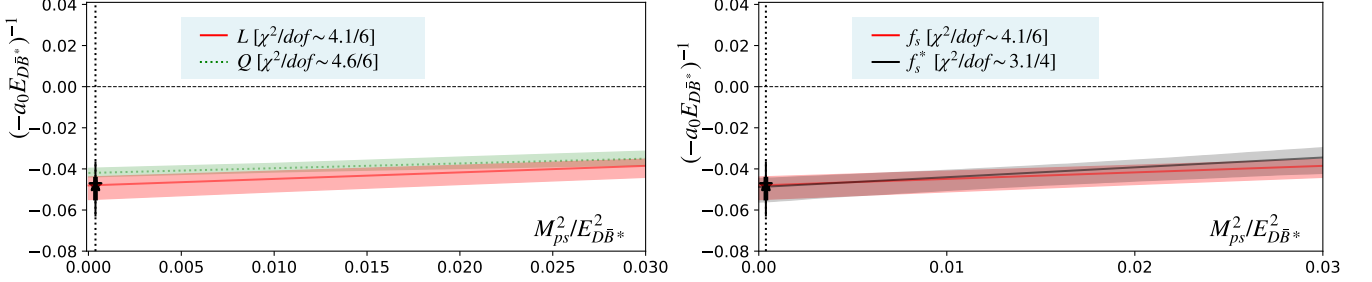


FIG. 5. Left: Comparison of light quark mass dependence of scattering amplitudes in the chiral regime determined from a linear (red band) and quadratic (green band) dependence of $kcot\delta_0$ on the lattice spacing. Right: Comparison of light quark mass dependence of scattering amplitude $kcot\delta_0$ in the chiral regime determined using the results from all five light quark masses (red band) and the results from four light light quark masses (black). The results in the physical limit in either cases can be seen to be consistent with the main result indicated by the star symbol.